Appl. Phys. B 70, 521–525 (2000) / Digital Object Identifier (DOI) 10.1007/s003400000212

Applied Physics B
Lasers
and Optics

Operation characteristics of the Au-II 690-nm laser transition in a segmented hollow-cathode discharge

G. Bánó[1], L. Szalai[1], K. Kutasi[1], P. Hartmann[1], Z. Donkó[1], K. Rózsa[1], Á. Kiss[1], T.M. Adamowicz[2]

[1] Research Institute for Solid State Physics and Optics, Hungarian Academy of Sciences, P.O. Box 49, H-1525 Budapest, Hungary
(E-mail: bano@sunserv.kfki.hu)
[2] Institute of Micro- and Optoelectronics, Warsaw University of Technology, Koszykowa 75, 00-662 Warsaw, Poland

Received: 1 July 1999/Revised version: 4 November 1999/Published online: 23 February 2000 –

Abstract. Single-mode operation at the Au-II 690-nm transition was obtained in a segmented hollow-cathode discharge laser without the use of any additional frequency-selective device. The pressure of the helium buffer gas, which is responsible for the significant homogeneous broadening of the laser line, was varied between 10 and 20 mbar. The discharge was excited with rectangular current pulses (up to 3 A) six times exceeding the threshold value. The time dependence of the laser output during the 1-ms-long discharge pulses is explained on the basis of the temperature and pressure changes in the tube. The highest small-signal gain at optimal discharge conditions was 11%m^{-1}.

PACS: 42.55.Lt; 42.60.Lh; 52.80.-s

Hollow-cathode metal ion lasers producing the metal vapor by cathode sputtering have been investigated for more than twenty-five years. The lasers usually employ helium or neon as buffer gas and copper, zinc, silver, aluminium or gold is used as cathode material [1]. The upper laser level is in most cases pumped by thermal-energy charge transfer reaction between buffer gas ions and metal atoms. Using special high-voltage discharge configurations [2] better performance could be reached on several transitions from the IR to the UV region compared to classical hollow-cathode arrangements. Usually buffer gas pressures in the range of 5–25 mbar are used in hollow-cathode tubes resulting in a significant pressure broadening of the laser lines. Therefore, as it was predicted in [3] single-longitudinal-mode operation is often an inherent feature of these lasers [4, 5]. This can be an advantage compared to other systems where a more complicated setup is needed to achieve single-mode operation, since the use of internal mode selectors always results in a reduced output power. Laser action at the Au-II 690-nm and 282-nm lines was first published in [6]; however, the identification of the 690-nm transition was given only twenty years later in [7]. Measurements using segmented hollow-cathode (SHC) discharge to pump the Au-II 282-nm UV laser line were reported in [8]. We investigated the He-Au laser system in the same SHC discharge arrangement. Our results obtained at the 282-nm transition were published elsewhere [9]. In this paper we present measurements on the operation of the 690-nm Au-II transition. To our best knowledge the small-signal gain measurements given here are also first data published for this line. The performance of the red line can possibly give us additional information about the UV transition of the Au-II laser, which has a similar pumping mechanism and discharge parameters.

1 Experimental

The experimental arrangement used in our measurements is depicted in Fig. 1. Six SHC modules each 5.6 cm long with inner diameter of 3.2 mm and separated with additional anodes formed the laser tube. The cross section of the modules can also be seen in Fig. 1. The electrodes were made of copper and the active areas of the cathodes were gold plated to a thickness of $\approx 30\,\mu$m. Two of the modules were placed 30 cm apart from the rest of the tube. In this way we made their operation independent from the others, which was important for the gain measurements. The tube had Brewster windows made of Suprasil quartz. The laser was operated in helium buffer gas with a small amount of argon to enhance the cathode sputtering. A pair of contra-rotating quartz plates within the resonator served as a variable loss element in the gain measurements. The length of the resonator was 140 cm. Two different sets of mirrors with curvature of 2 m and 3 m were used, having reflectance of $\approx 99\%$ and $\approx 100\%$, respectively. The laser output power was measured using a Hama-

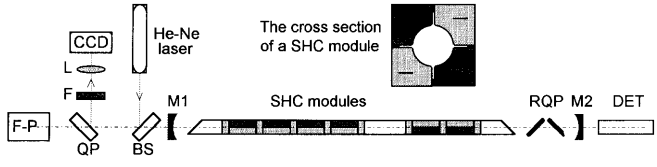

Fig. 1. The experimental setup and the cross section of a SHC module. M1, M2 – resonator mirrors, RQP – contra-rotating quartz plates, BS – beam-splitter, QP – quartz plate, F-P – Fabry–Pérot interferometer, F – filter, L – lens

matsu PIN diode calibrated with a Spectra-Physics 404 Power Meter. The signal from the opposite side of the resonator entered a Tec-Optics SA2 scanning Fabry–Pérot interferometer used for measurements of axial modes. The interferometer's resolution was suitable to resolve the longitudinal modes of the resonator separated by $\nu_F = c/2L = 107$ MHz. A He-Ne laser with a known mode separation was used to calibrate the dispersion of the interferometer. The signal could be directed to a CCD camera by means of a quartz plate and a lens. A filter was used here to weaken the intensity. The intensity distribution in the cross section of the beam observed by the camera gave information about the transverse modes of the laser. The discharge was excited by $\approx$ 1-ms-long rectangular current pulses at 1 Hz repetition rate to avoid heating and cathode erosion problems. The pulses were synchronised to the sweep frequency of the Fabry–Pérot interferometer.

2 Results and discussion

Typical voltage–current characteristics of the discharge are shown in Fig. 2. Voltages in the range of 400–800 V were applied for linear current densities up to 0.1 A cm^{-1}. The high slope resistance which is characteristic for high-voltage hollow-cathode configurations increases the stability of the discharge.

The effect of argon on the performance of sputtered metal ion lasers was studied in detail in [10] and recently in [9]. In this work the optimum argon admixture concentration for laser operation at the 690-nm wavelength was determined by measuring the dependence of the threshold current on the argon concentration. The results are shown in Fig. 3. Mirrors having curvature of 2 m formed the resonator here. The lowest threshold was obtained with 1% argon in the helium buffer gas and so this mixture was used in the following measurements. Threshold currents obtained with five SHC modules while using the 3-m-curvature mirrors and 1% argon can also be seen in Fig. 3.

To identify the lasing transition the spectrum of the spontaneous radiation from the discharge was recorded in the vicinity of the laser line and was compared with the spectrum obtained when the laser was operating. The spectra are plotted in Fig. 4.

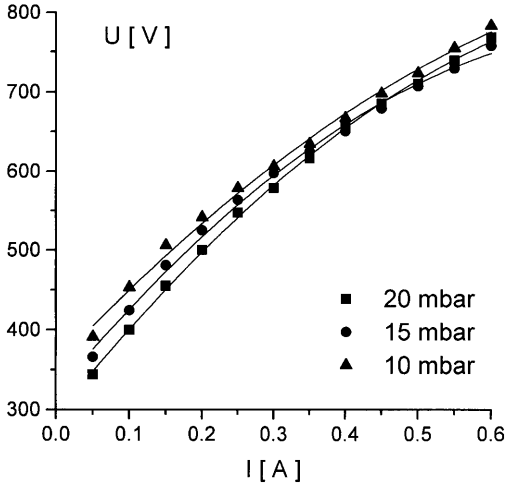

Fig. 2. Discharge voltage as a function of the current measured for one 5.6-cm-long SHC module with 1% of Ar in the He buffer gas

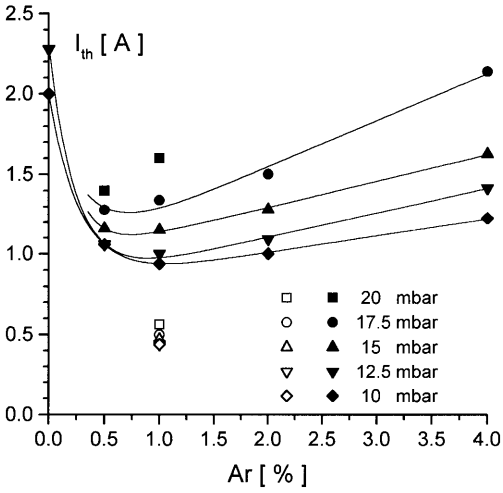

Fig. 3. Threshold current as a function of argon concentration. *Solid symbols* belong to results obtained with mirrors having curvature of 2 m while six SHC modules formed the active region. *Open symbols*: 3-m mirrors and five modules

Checking the intensity distribution of the laser beam in the transverse plane with the CCD camera and carrying out the spectral measurements with the Fabry–Pérot interferometer the following results were obtained. We found that using the 3-m-curvature mirrors the laser was only working in the transverse TEM$_{00}$ mode without the necessity of an additional diaphragm in the resonator. Furthermore, stable operation in a single longitudinal mode was observed in the investigated pressure range from 10 to 20 mbar for discharge currents up to 3 A (five SHC modules were used here). The intensity profile of the laser beam obtained for total discharge current $I = 3$ A at pressure $p = 17.5$ mbar can be seen in Fig. 5a. The corresponding spectrum of the laser line is shown in Fig. 5b covering two free spectral ranges of the interferometer. In

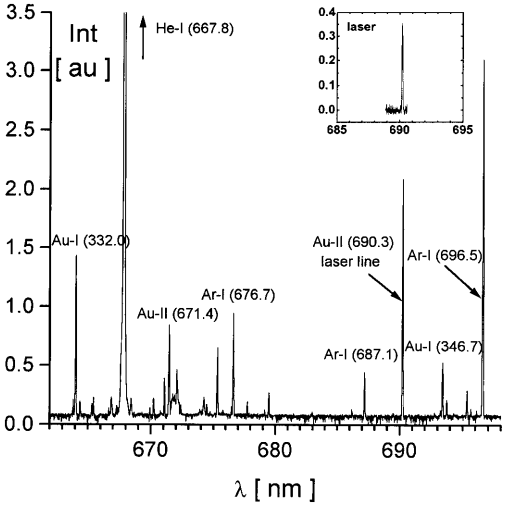

Fig. 4. Spectrum of the spontaneous emission of the laser tube with the identification of the most important transitions (wavelength given in nm units). Some of the lines originate from the second-order spectrum of the spectrograph. The *inset* shows the spectrum recorded while the laser was operating

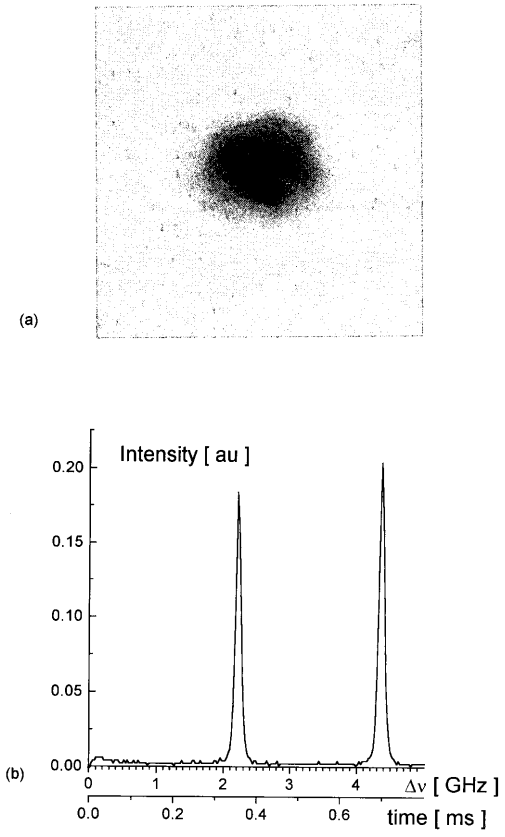

Fig. 5. a Intensity distribution in the cross section of the beam. **b** Frequency spectrum of the laser obtained with 3-m mirrors. ($p = 17.5$ mbar, $I = 3$ A)

certain mirror positions another weak longitudinal mode separated from the main peak by frequency of $2\nu_F$ appeared in the spectrum for single shots. However, the operation of this mode was very unstable and its intensity never exceeded 10% of the main peak. Assuming that for $I = 3$ A the gas temperature in the tube is approximately $T \cong 600$ K [11] the FWHM of the Doppler broadening is $\Delta\nu_D \cong 540$ MHz. Thus for this current (six times exceeding the threshold value) the laser should work in approximately seven different longitudinal modes unless a considerable homogeneous broadening is present.

The homogeneous broadening of the laser line can be obtained as the sum of the natural and the pressure broadening. Using the values of the calculated oscillator strength given in [7] for all the transitions originating from the upper and lower laser levels we obtain an approximation of the natural linewidth, $\Delta\nu_N \cong 110$ MHz. To get an idea about the importance of the pressure broadening the gain profile was calculated for the case of a single laser mode operating at the line centre. The shape of the hole burned into the gain profile was obtained from the exact expression given in [12] assuming the above value of the natural linewidth and different values of pressure broadening. Both the depth and the width of the hole depend on the intensity of the laser light. The effect of the laser intensity was adjusted to fulfill the requirement that the gain at the line centre is reduced to its threshold value. The second axial mode (observed experimentally) was supposed to start in the vicinity of the maxima appearing on the gain profile. We found that for typical conditions of our measurements the frequency difference between the maxima and the line centre varies between 200 and 250 MHz for pressure broadening in the range of $\Delta\nu_P = 0$–200 MHz. This is in agreement with the experimentally observed spectrum where $2\Delta\nu_F = 214$ MHz was found. It follows that from the frequency difference of the two working modes we cannot directly obtain the magnitude of the pressure broadening. Nevertheless, the maximum gain depends strongly on the assumed value of the pressure broadening. The maxima are more than twice above the threshold with no pressure broadening and drop to only 5% above the threshold for $\Delta\nu_P = 200$ MHz. Our experiments indicate that the gain is possibly low at the frequency of the second mode and this – taking into account the above calculations – shows that the pressure broadening causes a significant contribution to the homogeneous broadening. It is known that a laser mode working on a certain frequency will burn a hole into the gain profile also on the frequency placed symmetrically with respect to the line centre. From this we can conclude that in our case the two longitudinal modes (having same polarization due to the Brewster windows) and separated by $\Delta\nu = 2\nu_F$

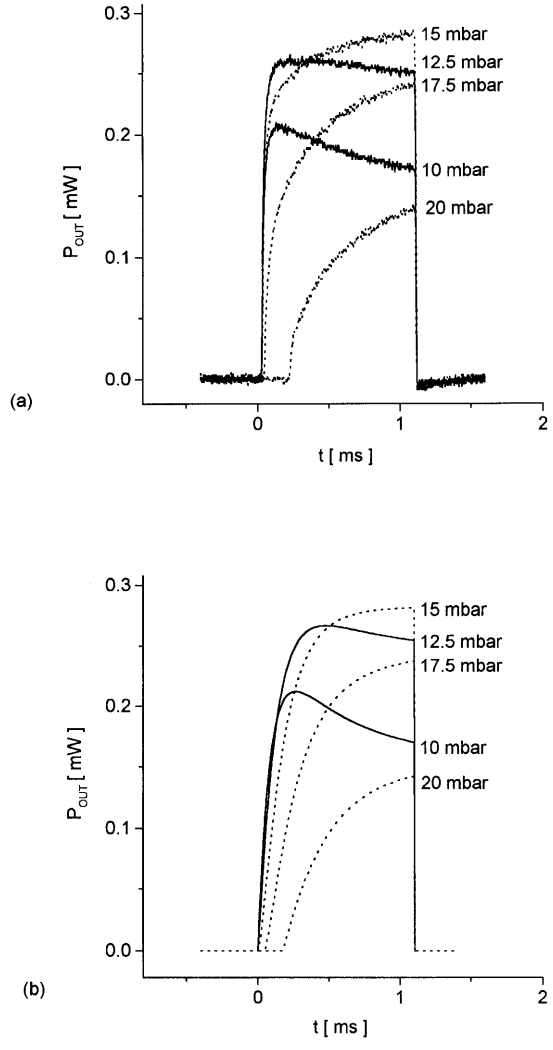

Fig. 6a,b. Time dependence of the laser output power obtained at different buffer gas pressures for $I = 2$ A (five modules were used). **a** Measured data. **b** Results of the model

could deplete the whole gain profile not allowing any other modes to start.

The time dependence of the laser output power for different pressures is shown in Fig. 6a. The resonator was not optimized for the maximum output power because of the lack of proper output coupler. It can be seen that at $p \leq 15$ mbar the laser operation starts $\approx 30\,\mu$s after the discharge is switched on. This can be explained by the diffusion of the sputtered gold atoms towards the tube centre. According to data published in [13] and assuming that the sputtering is mainly caused by Ar ions we can say that Au atoms are leaving the surface with an average energy of $E \cong 12$ eV. The thermalising range of sputtered particles $R(E)$ can be obtained from the theory of slowing down given in [14]. For $p = 15$ mbar it gives $R(12\,\text{eV}) = 0.3$ mm showing that gold atoms are thermalized relatively close to the cathode wall. Consequently, the sputtered atoms reach the centre of the tube due to their diffusive motion, which explains the delay of the laser action at lower gas pressures.

However, at higher pressures an unexpected time lag appears before the onset of the laser oscillation. It can be also seen from Fig. 6a that there is an optimum pressure $p \cong 15$ mbar for which the highest output power can be reached. For pressures below 15 mbar the laser intensity drops towards the end of the pulse whereas the opposite is true for higher pressures. This behaviour can be explained as follows. It is known (see for example [15]) that in continuously excited cathode sputtered metal ion lasers, an optimum pressure for each discharge current can be found for which the output is the highest. Assuming an approximately constant temperature for these conditions we can say that the pressure of the buffer gas is proportional to its density. Therefore, it seems to be likely that it is the density of the buffer gas that has to be optimized. The buffer gas density in our tube is decreasing during the discharge pulse due to the increased temperature in the active region, which can explain the time dependencies of the output power. For pressures higher than 15 mbar the initial density is above its optimum value. During the pulse it drops toward the optimum value resulting in a gradual increase of the output power. At 15 mbar the density remains in the vicinity of the optimum and finally at lower pressures it drops below the optimum resulting in a decrease of the power. The observed characteristic time constant of the changes is in the range of $\tau \cong 0.4$–1.3 ms. Extrapolating the measured data of the output power towards longer times we obtain an approximation of the output power (for $I = 2$ A) as a function of pressure in the case of continuously excited laser. Results are shown in Fig. 7; the fitted curve was used in the following calculations. To support the idea described above we calculated the rates of pressure and temperature changes in our tube. The time dependence of the gas temperature T_g is described by the expression [16]:

$$\frac{\partial}{\partial t}\left(\frac{3}{2} N k T_\text{g}\right) = \nabla \cdot \lambda_\text{g} \nabla T_\text{g} + H \,, \tag{1}$$

where N represents the concentration of He atoms, λ_g is the temperature-dependent gas thermal conductivity and H is the source term which includes the heating due to elastic collisions of neutral atoms with electrons in the negative glow and with ions in the cathode sheath. Assuming that the temperature profile in the tube is of parabolic shape and approximating the thermal conductivity with its mean value, the characteristic time of temperature changes is $\tau_T \approx 0.01$–0.02 ms. Despite this short response time of temperature changes, the pressure does not reach its equilibrium as rapidly in our narrow tube. As the temperature increases when the discharge is switched on, the pressure in the active region will be locally increased as well. We assumed in the following that the remaining parts of the tube (having much bigger volume compared to the discharge region) act as a reservoir with constant pressure. The time dependence of the pressure in the tube was calculated numerically on the basis of the conductance G of a narrow tube in viscous regime:

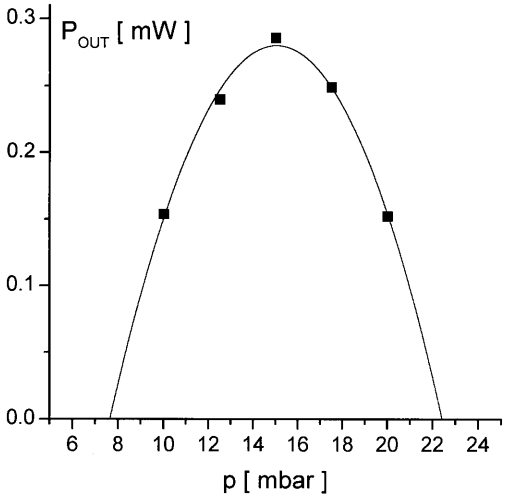

Fig. 7. Output power as a function of pressure obtained by the extrapolation of the measured curves (Fig. 6a) towards longer times

$$G = p\frac{\pi\, d^4}{128\, \eta_\text{g}\, L} \,, \tag{2}$$

where η_g is the gas viscosity, p is the pressure, d and L are the tube diameter and length, respectively. Afterwards the average pressure in the active region was used to get an approximation of the time-dependent output power according to the fitted curve in Fig. 7. Finally, the effect of the diffusion of the gold atoms was included in the model as a multiplication factor exponentially rising to unity. Results are depicted in Fig. 6b. A reasonably good agreement was obtained between the modelled and experimentally observed curves indicating that the main processes present in the tube were described properly. The 0.1-ms-long initial peak in the current pulse exceeding 1.3 times its equilibrium value could mainly cause the steeper rise of the measured data.

To measure the small-signal gain of the laser transition the tube was divided into two parts (oscillator and amplifier) excited by two independent (but synchronised) power supplies. The detailed description of the applied technique is given in [8]. First the current in the oscillator was adjusted to bring the laser to threshold. In this way the overall losses of the resonator were compensated. The desired current was then established in the amplifier resulting in an increase of the output power. Finally, the loss element was adjusted to re-establish threshold operation. The gain per pass for the amplifier was then equal to the additional loss inserted by the quartz

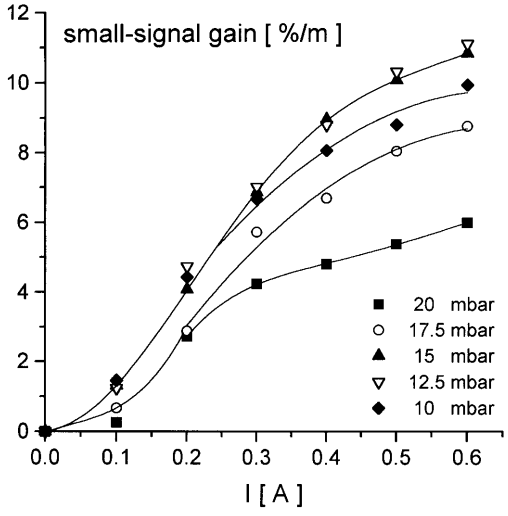

Fig. 8. Small-signal gain as a function of discharge current on a single module at different pressures

plates, which could be calculated using the proper Fresnel formula. The results of the measurements are shown in Fig. 8. The maximum value of the small-signal gain is $11\%\mathrm{m}^{-1}$ at $p = 12.5$ mbar and $I = 0.6$ A on a single SHC module.

3 Summary

We have shown that, due to the considerable homogeneous broadening the Au-II 690-nm segmented hollow-cathode discharge laser works in a single longitudinal mode in the pressure range between 10 and 20 mbar. The time needed to reach stable output power after switching the discharge on ($\tau \cong 0.4$–1.3 ms) was explained on the basis of temperature and pressure changes in the tube. The highest small signal gain was found to be $11\%\mathrm{m}^{-1}$ for optimum discharge conditions.

Acknowledgements. The authors would like to thank M. Jánossy and A. Gallagher for helpful discussion, T.J. Forgács, J. Tóth, E. Sárközi and Gy. Császár for technical assistance and acknowledge the support of the Hungarian Science Foundation (grants F-25530, T-25941 and T-25989).

References

1. D.C. Gerstenberger, R. Solanki, G.J. Collins: IEEE J. Quantum Electron. **QE-16**, 820 (1980)
2. K. Rózsa: Z. Naturforsch. **35a**, 649 (1980)
3. J.R. McNeil, G.J. Collins, F.J. DeHoog: J. Appl. Phys. **50**, 6183 (1979)
4. L. Csillag, C. Zong Nam, M. Jánossy, K. Rózsa: Opt. Commun. **21**, 39 (1977)
5. G. Xu, K. Fujii, S. Nakayama, A. Honma, Y. Uchiyama, Y. Tokita, Y. Hanazawa: Jpn. J. Appl. Phys. **36**, 129 (1997)
6. R.D. Reid, J.R. McNeil, G.J. Collins: Appl. Phys. Lett. **29**, 666 (1976)
7. M. Rosberg, J.F. Wyart: Phys. Scr. **55**, 690 (1997)
8. K.A. Peard, R.C. Tobin, K. Rózsa, Z. Donkó: IEEE J. Quantum Electron. **QE-30**, 1181 (1994)
9. L. Szalai, T.M. Adamowicz, A. Tokarz, G. Bánó, K. Kutasi, Z. Donkó, K. Rózsa: In OPTIKA '98: 5th Congress on Modern Optics, Proc. SPIE **3573**, 28 (1998); L. Szalai et al., to be published
10. H.J. Eichler, W. Wittwer: J. Appl. Phys. **51**, 80 (1979)
11. R.R. Arslanbekov, R.C. Tobin: J. Appl. Phys. **81**, 554 (1997)
12. W.R. Bennett, Jr.: *The Physics of Gas Lasers* (Gordon & Breach, New York 1973)
13. R.V. Stuart, G.K. Wehner, G.S. Anderson: J. Appl. Phys. **40**, 803 (1969)
14. A. Gras-Marti, J.A. Valles-Abarca: J. Appl. Phys. **54**, 1071 (1983)
15. J.R. McNeil, W.L. Johnson, G.J. Collins, K.B. Persson: Appl. Phys. Lett. **29**, 172 (1976)
16. M.J. Kushner, B.E. Warner: J. Appl. Phys. **54**, 2970 (1983)